

HUBBLE SPACE TELESCOPE WFPC2 IMAGING OF THREE LOW SURFACE BRIGHTNESS DWARF ELLIPTICAL GALAXIES IN THE VIRGO CLUSTER

KAREN O'NEIL¹

Arecibo Observatory, HC3 Box 53995, Arecibo, PR 00612; koneil@naic.edu

G. D. BOTHUN

Department of Physics, University of Oregon, Eugene, OR 97403; nuts@bigmoo.uoregon.edu

AND

C. D. IMPEY

Steward Observatory, University of Arizona, Tucson, AZ 85721; impey@as.arizona.edu

Received 1998 April 7; accepted 1999 June 14

ABSTRACT

Utilizing the F814W and F300W filters, *Hubble Space Telescope* Wide Field Planetary Camera 2 (WFPC2) images were taken of three low surface brightness dwarf elliptical galaxies in the Virgo Cluster. The intent of the observations was to determine the small-scale structure in these enigmatic galaxies and to attempt to learn something about the nature of their giant branches through the detection of luminosity fluctuations. In two of the three studied galaxies, V7L3 and V1L4, the luminosity fluctuations in the inner, constant surface brightness regions were unambiguously detected. At the nominal distance of the Virgo Cluster, the measured luminosity fluctuations in the F814W band yields a density of 2–10 red giants per pixel. In the most extreme of these two cases, V7L3, we derive a surface density of giant stars of ~ 3 per 10 pc^2 . Using the observed $B-V$ and $V-I$ colors as a constraint, we could find no model that would reproduce the observed fluctuation signal and blue colors if there were a significant population of M giants in these systems. Overall, our results are consistent with a mean spectral type of K0–K2, which implies a relatively metal-poor population. The third system, V2L8, did not have a detectable fluctuation signal, which possibly implies that it is not in the Virgo Cluster. Interestingly, this system is highly nucleated. Our observations have resolved this nucleus, and if V2L8 is in Virgo, then we have discovered what is likely the smallest bulge measured to date, having an effective radius of only 50 pc. This bulge is quite red (as red as giant ellipticals), and it is entirely possible that this nucleated dwarf elliptical galaxy, in fact, is a very large galaxy located in the background. As such, it is highly reminiscent of the manner in which Malin 1 was discovered. Optical spectroscopy of this nucleus is required to confirm this. Finally, we find no evidence for small-scale clumping of stars in any of the studied systems at this much-improved spatial resolution. This implies that these systems are dynamically well relaxed and that the physical cause of their observed low surface brightnesses is their low density. When imaged at the high spatial resolution of the WFPC2 ($\sim 6 \text{ pc pixel}^{-1}$), the galaxies are easy to look right through without even knowing that they are present in the very middle of the WFPC2 frame. They appear only as elevated “sky noise.”

Key words: galaxies: dwarf — galaxies: evolution — galaxies: individual (V1L4, V2L8, V7L3) — galaxies: statistics — galaxies: stellar content — galaxies: structure

1. INTRODUCTION

Little is known or understood about the current stellar populations and/or star formation histories of low surface brightness (LSB) dwarf elliptical (dE) galaxies. What we do know from various studies (e.g., Sung et al. 1998; Jerjen & Dressler 1997; Secker & Harris 1996; Durrell et al. 1996; Meylan & Prugniel 1994; Lee, Freedman, & Madore 1993; Peterson & Caldwell 1993; Impey, Bothun, & Malin 1988; Caldwell 1987; Caldwell & Bothun 1987; Bothun et al. 1985, 1986; Kormendy 1985, 1987; Bothun & Caldwell 1984) can be summarized as follows (see Ferguson & Bingelli 1994 for a fuller review):

1. LSB dE's in the Virgo and Fornax clusters generally define a tight surface brightness–magnitude relation (Secker & Harris 1996). This relation is driven by the tendency for dE surface brightness profiles to be extremely well fitted by an exponential function, coupled with a near-constancy of

the disk scale length ($\alpha \sim 0.9 \pm 0.1 \text{ kpc}$; see Bothun, Caldwell, & Schombert 1989; Caldwell & Bothun 1987; Young & Currie 1995). Thus, variations in luminosity are driven solely by variations in central surface brightness. In a simple universe there would also be a corresponding color versus surface brightness relation, with the lower luminosity dE's being redder than the higher luminosity ones. This would make the surface brightness–magnitude relation merely a fading sequence. Naturally, things are more complicated than this, as no color–central surface brightness relation has been observed for any sample. In fact, the available data actually define a relation in the opposite sense, namely, dE's with the lowest central surface brightness are the bluest (see Fig. 3 in Bothun, Impey, & Malin 1991).

2. There is a small but important component of very LSB dE's with large scale lengths that strongly deviate from the standard surface brightness–magnitude relation (see Impey, Bothun, & Malin 1988; Bothun et al. 1991; Caldwell et al. 1998; O'Neil 1997). Although there is no difference in mean color, these very diffuse dE's may be fundamentally different than the other dE's. Some of the more extreme

¹ Work was done while at the University of Oregon.

examples in this class reach central surface brightnesses as low as $\mu_B(0) = 26.0$ mag arcsec $^{-2}$ but have scale lengths of ~ 1.5 kpc.

3. An appreciable fraction of LSB dE's have conspicuous nuclei. Spectroscopy (e.g., Bothun & Mould 1988; Brodie & Huchra 1991; Peterson & Caldwell 1993; Held & Mould 1994) indicates a stellar population similar to that of metal-rich Galactic globular clusters but with stronger Balmer line equivalent widths, perhaps indicating a lower mean age. In general, there is little difference in color between most nuclei and the surrounding envelope. Whether these nuclei are minibuclges (e.g., $r^{1/4}$ components) or the site of a secondary star formation event is currently unclear.

4. Most dE's have little neutral hydrogen, suggesting that substantial gas loss may have occurred as the result of baryonic blowout in shallow potentials because of energy input from supernovae (e.g., Dekel & Silk 1986; Vader 1987; Silk, Wyse, & Shields 1987; Spaans & Norman 1997).

5. While some possible "transition" objects have been identified on their way to becoming gas-poor dE's (e.g., Meurer, Mackie, & Carignan 1994; Knezek, Sembach, & Gallager 1997; Vader & Chaboyer 1994; Sage, Salzer, & Loose 1992; Conselice & Gallagher 1998), it is fairly unclear what their present evolutionary nature is. Only a handful of these candidate transition galaxies exist, compared with the relatively large numbers of dE's in clusters, suggesting that whatever evolutionary process has produced dE's is no longer ongoing with much frequency.

6. The number density of dE's in groups and clusters seems to be correlated with the total cluster luminosity in the sense that large, brighter clusters (e.g., Virgo) have significantly more dE's than fainter clusters such as Fornax (see Ferguson 1991; Secker & Harris 1996). This is a compelling result that strongly suggests some quite macroscopic physical event is responsible for the production of dE's in clusters. Indeed, very deep studies of the Coma Cluster suggest that there may be thousands of dE's in that environment (Ulmer et al. 1996; Bernstein et al. 1995; Secker, Harris, & Plummer 1997).

Missing from the above list is any explanation as to why the surface brightnesses of these dE's can be so low at a wide range of $B-V$ and $V-I$ colors. Surface brightness is, of course, a convolution of the average separation between the stars and the luminosity function of the stars in the galaxy. Broadly speaking, the available photometric data on dE's are inconsistent with a significant change in the stellar luminosity function—that is, the broadband integrated colors, as well as nuclear spectra, indicate the light is dominated by a giant branch augmented by A, F, and G main-sequence stars. Given this, the most probable reason that these galaxies have such low surface brightnesses is a larger than average separation between the stars or between individual red giants in the case of giant dominated integrated light. Is this a formation effect? That is, have these systems always been of low-mass density (see de Blok & McGaugh 1997), or has there been some profound evolutionary process, perhaps associated with significant mass loss (e.g., Dekel & Silk 1986), that has "puffed" what once were compact galaxies into a considerably more diffuse state?

But what is the evidence, apart from general broadband colors, that the light from dE galaxies is giant dominated? As remarked by Bothun et al. (1991) and McGaugh, Schombert, & Bothun (1995), there is particular difficulty in fitting

stellar population models to the blue end of the LSB dE sequence because these objects are blue in the clear absence of ongoing star formation. In general, this end is defined by objects with $B-V \sim 0.4-0.5$ and $V-I \sim 0.6-0.8$. For these objects, their colors can be reproduced using a large population of A, F, and G stars and a reduced giant branch (which indicates a young mean age for the galaxy), thus bringing into question the statement that their light is giant dominated. One way to directly test whether these blue dE's still have giant dominated light is offered by the measurement of luminosity fluctuations using the *Hubble Space Telescope* (HST). Previous attempts to measure the fluctuation signal of LSB dE's from the ground have been successful. Bothun et al. (1991) successfully detected the B -band fluctuations in two LSB dE galaxies in Fornax using a detector with pixel size of $0''.33$ under conditions of $0''.7-0''.8$ seeing. Jerjen, Freeman, & Binggeli (1998) measured the R -band fluctuation signal for a few dE galaxies in Sculptor using a detector with pixel size of $0''.60$ under conditions of $1''.5$ seeing.

Clearly, at $0''.1$ pixel $^{-1}$ and a point-spread function (PSF) of approximately $0''.2$, HST observations using the Wide Field Planetary Camera 2 (WFPC2) present a unique opportunity for a robust measurement of the fluctuation signal from LSB dE's in structures as distant as the Virgo Cluster. A priori, what might one expect from such measurements? Well, suppose there is some dE with a region of constant surface brightness of $B = 25.0$ mag arcsec $^{-2}$ a few arcseconds in size. At I , the mean surface brightness will be approximately $I = 23.5$ mag arcsec $^{-2}$. At $0''.1$ pixel $^{-1}$, each WFPC2 pixel would have $B = 28.5$ mag. At the distance of the Virgo Cluster ($m-M = 31.5$ for this illustrative purpose only), the absolute magnitude per pixel in the I band is -3.0 . If the light per pixel is giant dominated then this absolute magnitude level is reached with just 2–10 giants, depending on their spectral type. The Poisson noise associated with such a discrete distribution of giants would indeed be large ($\geq 33\%$). If, on the other hand, the light from these blue dE's is dominated by F and G main-sequence stars, then several hundred per pixel are required and the corresponding fluctuation signal would be significantly reduced. We thus seek to determine the amplitude of the fluctuation signal in a small sample of blue LSB dE's in Virgo to (1) directly test that the light from these dE's is still giant dominated and (2) show membership in the Virgo Cluster.

Additional motivation for performing these observations is threefold. (1) There is conflicting information in the literature concerning the metal abundance and/or effective temperatures of the giant branches in these systems. For instance, the interpretation offered by Bothun & Mould (1988) is somewhat different than that put forth by Brodie & Huchra (1991). By measuring the fluctuation signal, we have an opportunity to infer the approximate K/M ratio in the composite giant branch. In globular clusters, it has been shown (Reed, Hesser, & Shawl 1988), that the K/M giant ratio is a good indicator of metallicity. (2) We know very little about the small-scale structure of these enigmatic dwarf galaxies. For instance, are these dE's of low surface brightness because the mean giant luminosity per pixel is low, or is the actual surface density of giants (absolute numbers of stars per pixel) low? Determining the luminosity fluctuations associated with discrete numbers of giants per pixel can help resolve this. (3) The nature of the nuclei that frequent many dE's in Virgo remains unclear.

One dE in our sample exhibits a very red nucleus that is spatially unresolved from the ground. WFPC2 observations may help to resolve this nucleus to better determine its nature.

In this paper, we describe our imaging experiment of three LSB dE's in Virgo. This experiment has never been tried before on Virgo dE's. Section 2 describes our dE sample, as well as the instrumentation and data reduction procedures. In § 3 we report on the detection of the fluctuation signal and present some model analysis on the nature of the composite giant branch in these systems. Section 4 gives a complete error analysis for the images, and § 5 discusses the nature of the individual dE's in more detail.

2. OBSERVATIONS AND DATA REDUCTION

2.1. The dE Sample: Global Properties

For this study, we selected three LSB dE's in Virgo from the ground-based Las Campanas 2.5 m dupont Telescope CCD sample of Impey, Bothun, & Malin (1988, hereafter IBM). Two of these three are in the Virgo Cluster catalog (VCC) of Sandage & Binggeli (1984). The objects chosen are V1L4 (VCC 1582), V2L8, and V7L3 (VCC 1149).

V1L4 is fairly easy to identify in the ground-based images, but the presence of a large number of (apparent) foreground stars makes analysis of this galaxy, at ground-based resolution, difficult. The extrapolated central surface brightness is $24.2 B \text{ mag arcsec}^{-2}$, and the integrated B magnitude is 16.7, making it the brightest of the three dE's in this study. The galaxy is circular in appearance, with the hint of a faint spiral arm on the northeastern side of the galaxy (much like the incipient spiral structure of Malin 1; see Impey & Bothun 1989). The surface brightness profile consists of a flat central region followed by an exponential falloff. This lack of a true exponential profile, to $R = 0$, prevents an accurate determination of scale length, but its $27.0 B \text{ mag arcsec}^{-2}$ isophote diameter suggests a scale length similar to the other two dE's in this study.

V2L8 has a central surface brightness of only $25.8 B \text{ mag arcsec}^{-2}$, making it the most diffuse object in this study (and explaining why it is not a VCC object). The galaxy is roughly circular in appearance but is well nucleated. Unfortunately, in the IBM data there is a CCD flaw running through the center of the galaxy that prevented much analysis of this nucleation. We have included this object in our sample in hopes of resolving the nucleation with *HST*. V2L8 nominally has a scale length slightly larger than the typical dE in Virgo or Fornax ($\alpha_{V2L8} = 1.2 \text{ kpc}$). When combined with the very low central surface brightness,

V2L8 is well outside the standard surface brightness–magnitude relation discussed in § 1.

V7L3 is intermediate between the other two. It has a measured central surface brightness of $25.1 \text{ mag arcsec}^{-2}$ and a scale length of $\alpha_{V7L3} = 1.1 \text{ kpc}$. Like V2L8, it too is an exception to the standard surface brightness–magnitude relation of dE galaxies. As will be seen, V7L3 was the most difficult galaxy to identify in the WFPC2 data because it is very diffuse and lacks any nucleation.

The light distribution of the three galaxies is remarkably similar. Once the bright nuclear core of V2L8 is removed, all three dE's have a flat inner surface brightness profile followed by an exponential profile that continues through the detection limit. It is in these flat diffuse regions that we seek to measure the fluctuation signal. These regions may be kept diffuse by the action of background radiation pressure, stellar winds, or some other mechanism that provides enough outward pressure to prevent an increase in density and reduction in scale size of these diffuse regions (i.e., Kepner, Babul, & Spergel 1997).

Information from the ground-based images is given in Table 1 and described below. All quantities were calculated using the Johnson B -band filter unless otherwise noted. It should be stated that although the images and zero points used for this table are the same as those used in IBM, the parameters have been independently calculated, by redoing the surface photometry.

Columns (1) and (2).—Galaxy names as given in IBM (col. [1]) and in the Binggeli, Sandage, & Tarenghi atlas (1985; col. [2]).

Columns (3) and (4).—Right ascension and declination of the galaxies, as found using the STSDAS METRIC task on the WFPC2 F814W images (J2000.0 epoch).

Column (5).—Central surface brightness, in mag arcsec^{-2} .

Column (6).—The scale length, in arcseconds, as defined in equation (2) below.

Column (7).—The total B magnitude integrated out to the $27.0 \text{ mag arcsec}^{-2}$ isophote.

Column (8).—The isophotal diameter measured at the $\mu_B = 27.0 \text{ mag arcsec}^{-2}$ level.

Columns (9) and (10).—The $B - V$ and $V - I$ colors, measured through the $d = 20''$ aperture for V2L8 and V1L4 and through the $d = 34''$ for V7L3, because of the difficulty in obtaining an accurate color at smaller apertures (see § 5). The errors are 0.05 and 0.1 for $B - V$ and $V - I$, respectively.

The colors of these dE's are fairly blue. For comparison, the typical Galactic globular cluster has colors of $B - V = 0.62 \pm 0.02$ and $V - I = 0.93 \pm 0.05$ ($[\text{Fe}/\text{H}] \leq -1.7$). It is likely that the stellar populations in these

TABLE 1
PHOTOMETRIC AND STRUCTURAL PROPERTIES OF THE THREE VIRGO GALAXIES
AS DETERMINED FROM GROUND-BASED IMAGES

Galaxy (1)	Name (2)	R.A. (3)	Decl. (4)	$\mu_B(0)$ (5)	α (arcsec) (6)	B_{27} (7)	D_{27} (8)	$B - V$ (9)	$V - I$ (10)
V1L4.....	VCC 1582	12 28 58.92	12 54 29.7	24.2 ^a	a	16.68	74	0.52	0.71
V2L8.....		12 34 42.30	14 13 22.4	25.78	20.1	18.33	51	0.46	1.10
V7L3.....	VCC 1149	12 28 58.98	12 54 28.3	25.07	19.1	17.72	60	0.38 ^b	0.79 ^b

NOTE.—Units of right ascension are hours, minutes, and seconds, and units of declination are degrees, arcminutes, and arcseconds.

^a No line was fitted to the exponential profile of the ground-based image, and the central surface brightness value is approximate.

^b These colors were found at $D = 37''$.

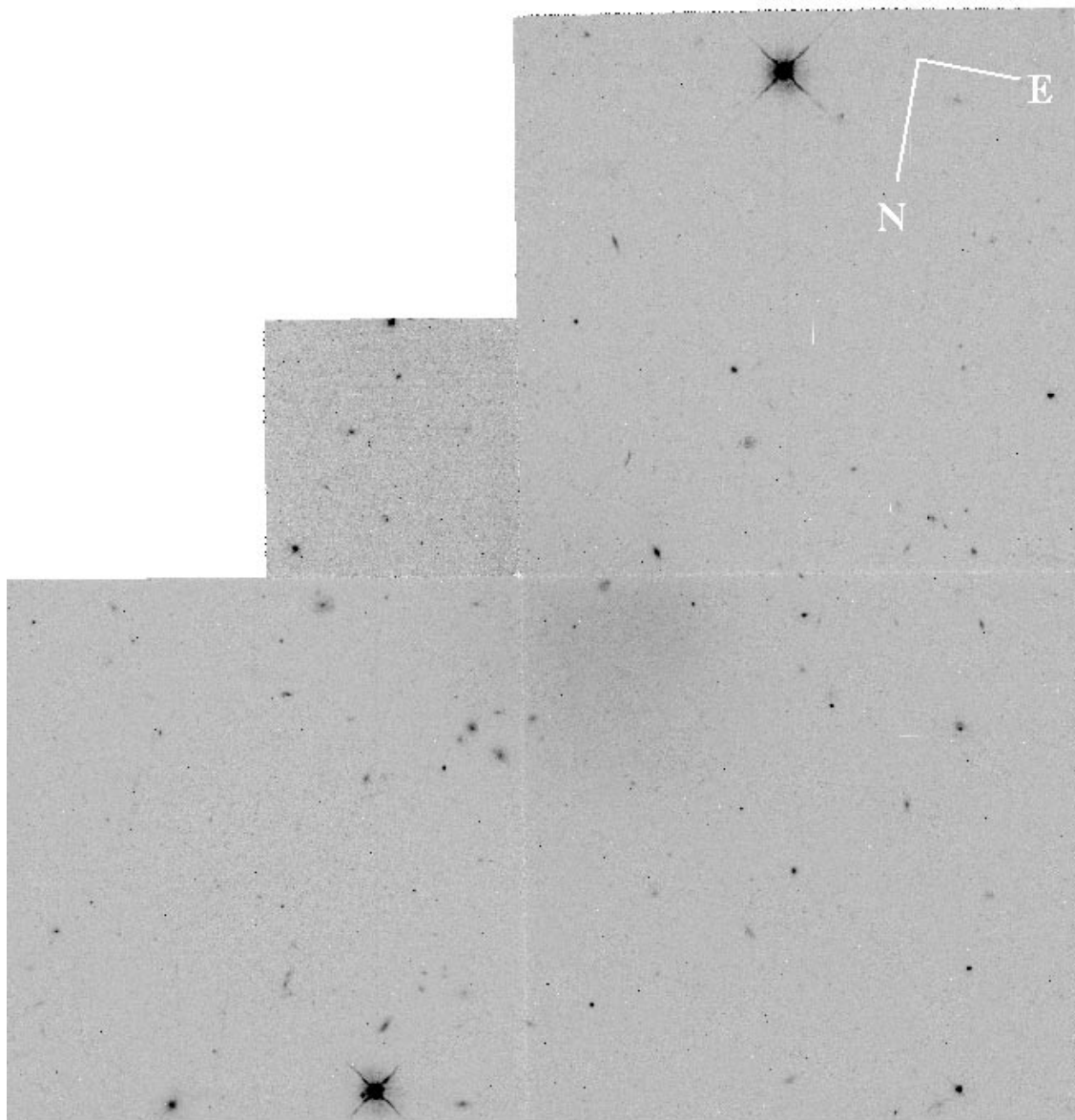


FIG. 1a

FIG. 1.—*HST* WFPC2 mosaicked images of (a) V1L4, (b) V2L8, and (c) V7L3 taken through the F814W (*I* band) filter with a 2200 s exposure time. These images are 2.6 arcsec across.

dE's are metal-poor, with a younger mean age than those found in Galactic globulars. This would imply a deficit of M giants, which is something that can be constrained from the measured fluctuation signal.

2.2. Instrumentation

The WFPC2 consists of three Wide Field Cameras and one Planetary Camera. The Wide Field Cameras have a focal ratio of $f/12.9$ and a field of view of $80'' \times 80''$, with each pixel subtending 0.0996 arcsec^2 . The three cameras form an L shape, with the Planetary Camera completing the square. The Planetary Camera has a focal ratio of $f/28.3$, $0.0455 \text{ arcsec}^2 \text{ pixel}^{-1}$, and an overall field of view of 36 arcsec^2 . All four cameras have an 800×800 pixel silicon CCD with a thermoelectric cooler to suppress dark current. The WFPC2 has two readout formats: single pixel resolution (FULL mode) and 2×2 pixel binning (AREA mode). The digital-to-analog converter used a gain of $7 e^-$ per digital number.

The data for this survey were acquired on 1996 May 1, August 3 and October 3. Each field was chosen so that the center of the dE was located in the WF3 image. Four images of each galaxy were taken using all four WF and PC chips, for a total of 2100 and 2200 s through the F300W and F814W filters, respectively. The F814W filter is a broadband filter with $\lambda_0 = 7924 \text{ \AA}$ and $\Delta\lambda_{1/2} = 1497 \text{ \AA}$. It is designed to be similar to the Cousins *I*-band filter. The F300W filter has $\lambda_0 = 2941 \text{ \AA}$ and $\Delta\lambda_{1/2} = 757 \text{ \AA}$ and is the WFPC2 wide-band U filter. The F814W images were taken in FULL mode, while the F300W images were taken in AREA mode. Because of the CCD response, the signal-to-noise ratio (S/N) through the F814W filter was considerably higher than through the F300W filter. Surface brightness profiles and structural parameters were all found through the F814W images. Figure 1 shows the full (mosaicked) images through the F814W filter.

Sky flat fields of the sunlit Earth were taken through each filter and routinely calibrated against an internal flat-field calibration system. The internal system consists of two

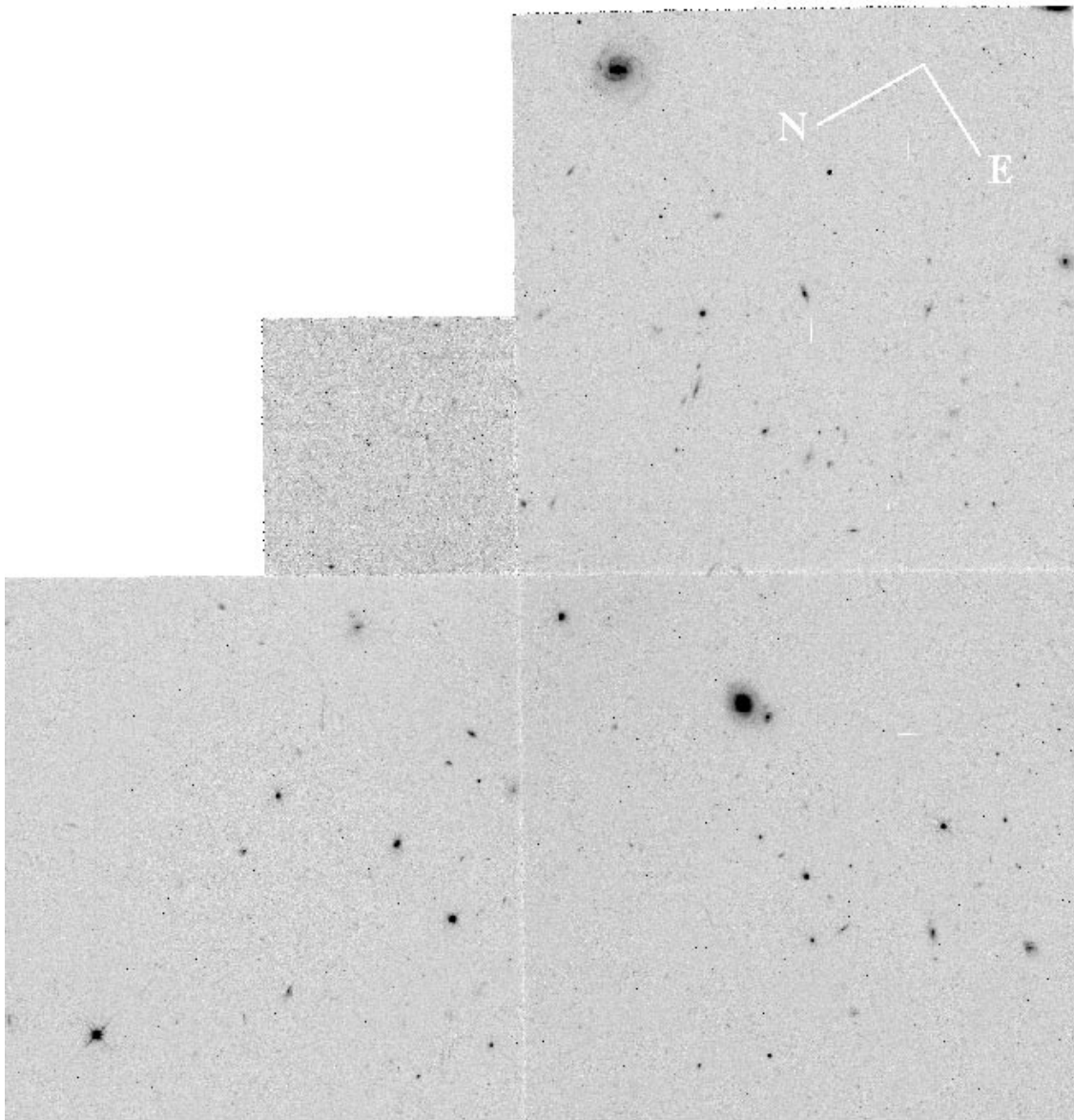


FIG. 1b

lamps (optical and UV) illuminating a diffuser plate. The internal flats are used to monitor and correct for changes in the flat fields. Dark fields are averages of 10 calibration frames taken over the space of 2 weeks. The intrinsic dark rate of the WFPC2 CCDs is $\leq 0.01 e^- \text{ pixel}^{-1} \text{ s}^{-1}$. A bias field was generated for each image using extended register pixels that do not view the sky.

The data reduction process was as follows: First, all known bad pixels were removed by use of the static mask reference file. The bias level was then removed from each frame. The bias image, generated to remove any position-dependent bias pattern, was then subtracted from the image, as was the dark-field image. Flat-field multiplication was then performed. All the above image calibration was performed at STScI using the standard WFPC2-specific calibration algorithms (the pipeline). After the images were reduced, they were inspected for obvious flaws, such as filter ghosts or reflections. As none were found, all the images were used in the subsequent analysis. Each frame was then shifted, registered, and combined by use of the STSDAS

CRREJ procedure to eliminate cosmic rays and other small-scale flaws. The resultant 2100–2200 s images were then checked by eye to ensure that any registration errors were less than 0.5 pixels.

2.3. Data Reduction

The zero points for each field were taken from the PHOTFLAM value given in the image headers. The zero point, in the STMAG system (the Space Telescope system based on a spectrum with constant flux per unit wavelength set to approximate the Johnson system at V), is $ZP_{\text{STMAG}} = -2.5 \log(\text{PHOTFLAM}) - 21.1$. For the F814W filter, the PHOTFLAM was 2.5451×10^{-18} , corresponding to a zero point of 22.886. For the F300W filter, the PHOTFLAM was 6.0240×10^{-17} , with a zero point of 19.450. Conversion to the Cousins I band was done using the value given in by Whitmore in the WFPC2 Photometry Cookbook of $F814W - I = 1.22 \pm 0.01$ (for objects with the colors of galaxies). Conversion from the F300W band to the Johnson U band is more complicated because of an

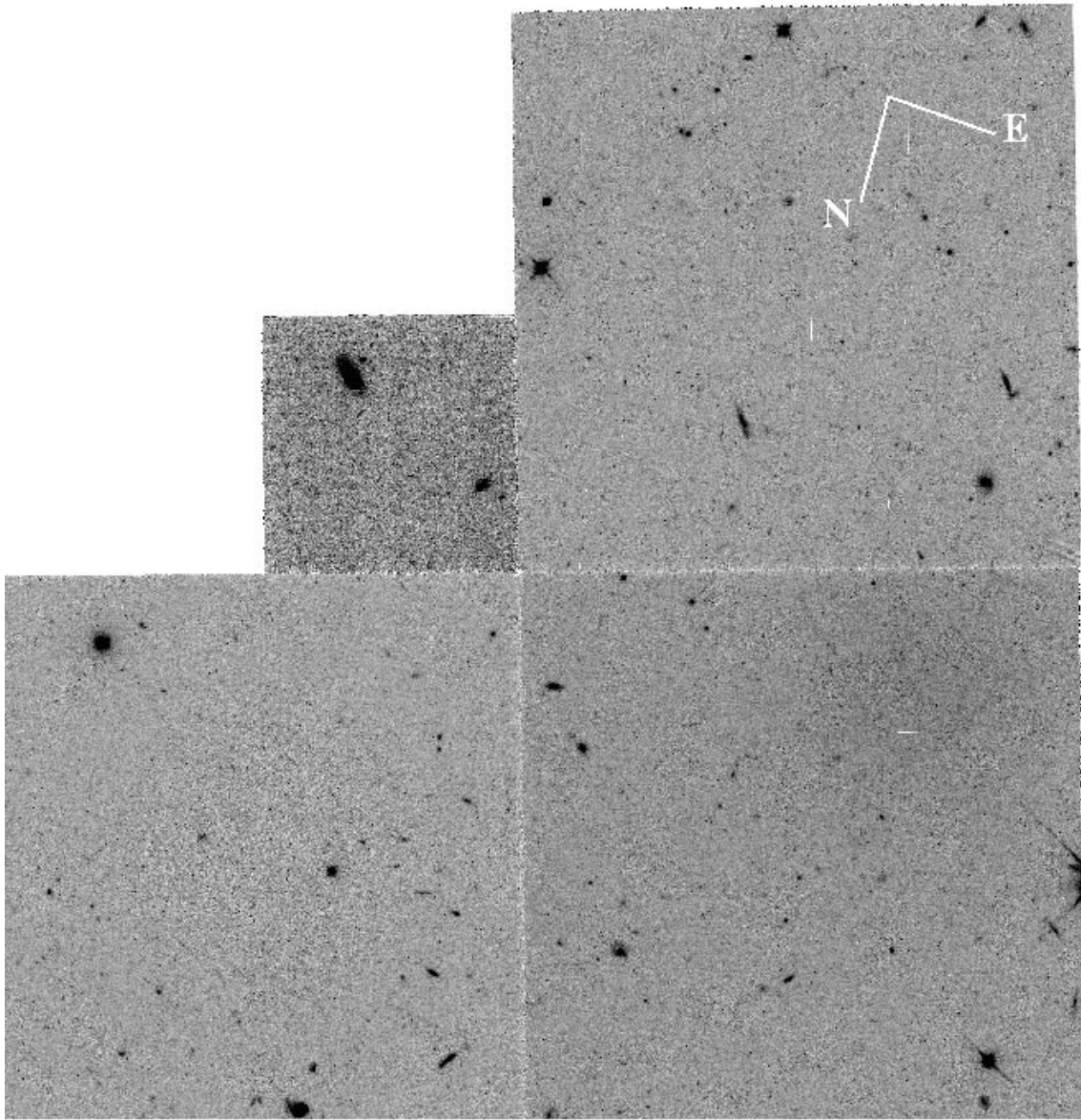


FIG. 1c

imperfect match between the filters. As a result, we used the value obtained by O'Neil et al. (1998) of $F300W - U = 0.004 \pm 0.1$.

The physical center of each galaxy, estimated by centroiding with respect to outer isophotes, was found, and ellipses were fitted around that point to obtain the intensity in each annulus using the modified GASP software (Cawson 1983; Bothun et al. 1987). The pixel size of the survey provides a seeing radius (stellar PSF) of $0''.1$ for the Planetary Camera and $0''.2$ for the Wide Field Cameras. The average sky-subtracted intensity within each (annular) ellipse was found and calibrated with the photometric zero point. Background galaxies were masked with the GASP software, which sets the value of the affected pixel to $-32,768$ and subsequently ignores the affected region.

Exponential surface brightness profiles were plotted against the major axis (in arcseconds) for each galaxy by use of the following equation:

$$\Sigma(r) = \Sigma_0 e^{-r/\alpha}, \quad (1)$$

where Σ_0 is the central surface brightness of the disk in linear units ($M_\odot \text{ pc}^{-2}$) and α is the exponential scale length in arcseconds. This can also be written (the form used for data analysis) as

$$\mu(r) = \mu(0) + (1.086/\alpha)r, \quad (2)$$

where μ_0 is the central surface brightness in mag arcsec^{-2} .

The average sky brightness through the F814W filter was $23.01 \text{ mag arcsec}^{-2}$ (which corresponds to about $21.8 \text{ mag arcsec}^{-2}$ in the Johnson *I*-band system). An accurate (error $\leq 0.25 \text{ mag arcsec}^{-2}$) radial surface brightness profile was typically found out to $25.5 \text{ mag arcsec}^{-2}$ (10% of the sky background).

3. DATA ANALYSIS AND MODELING

3.1. Measuring the Fluctuation Signal

The flat surface brightness profile in the inner core of these dE galaxies, combined with the exceptionally flat sky

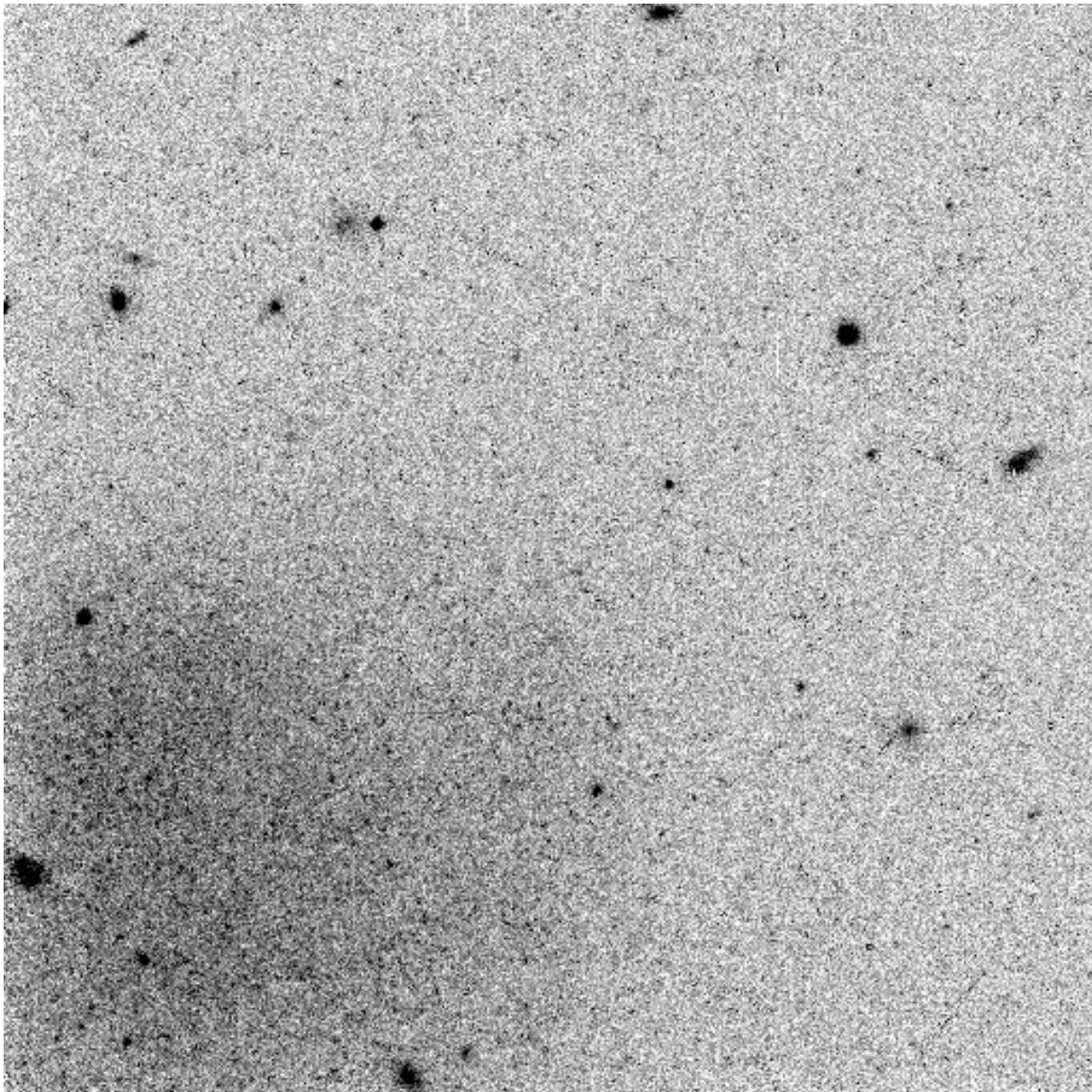


FIG. 2a

FIG. 2.—Nuclear regions of the three galaxies, V1L4, V2L8, and V7L3, respectively. These images are each $49''.8$ across.

background of our WFPC2 F814W images (flat to less than 0.1%), allows for an accurate detection of luminosity fluctuations caused by the stellar population of these inner regions. Figure 2 shows the gray-scale images for the inner regions of the galaxies in the F814W images. In all three cases the profiles are flat, with mean $\mu = 24.39, 26.23,$ and 25.49 F814W mag arcsec $^{-2}$ for V1L4, V2L8, and V7L3,

respectively. Pixel-to-pixel variations within the flat regions (as defined in Table 2, col. [2]), as well as for the sky, were then found by determining the mean electron count and dispersion in three sets of 135 boxes 5, 10, and 15 pixels wide, for a total of 47,250 pixels, which were spread randomly throughout the region of constant surface brightness (see also Bothun et al. 1991). Multiple random samplings

TABLE 2
LUMINOSITY FLUCTUATIONS FROM THE INNER REGIONS OF THE THREE GALAXIES

Galaxy (1)	Radii (arcsec) (2)	μ_{814} (mag arcsec $^{-2}$) (3)	μ_I (mag arcsec $^{-2}$) (4)	Galaxy (e^-) (5)	σ_{Galaxy} (e^-) (6)	Sky (e^-) (7)	σ_{sky} (e^-) (8)	Dispersion (e^-) (9)	\bar{M}_I (mag) (10)
V1L4.....	1.5–7.0	24.39	23.1	181.2 ± 0.8	21.7 ± 0.6	145.2 ± 0.3	18.4 ± 1.0	0.33 ± 0.05	–0.3 to 0.8
V2L8.....	6.0–25	26.23	25.0	179.2 ± 0.4	21.5 ± 0.6	169.4 ± 0.4	21.1 ± 0.8	0.65 ± 0.17	...
V7L3.....	1.0–10	25.49	24.2	169.1 ± 0.3	20.1 ± 1.0	154.5 ± 0.4	19.5 ± 0.5	0.65 ± 0.17	–0.54 to –1.04

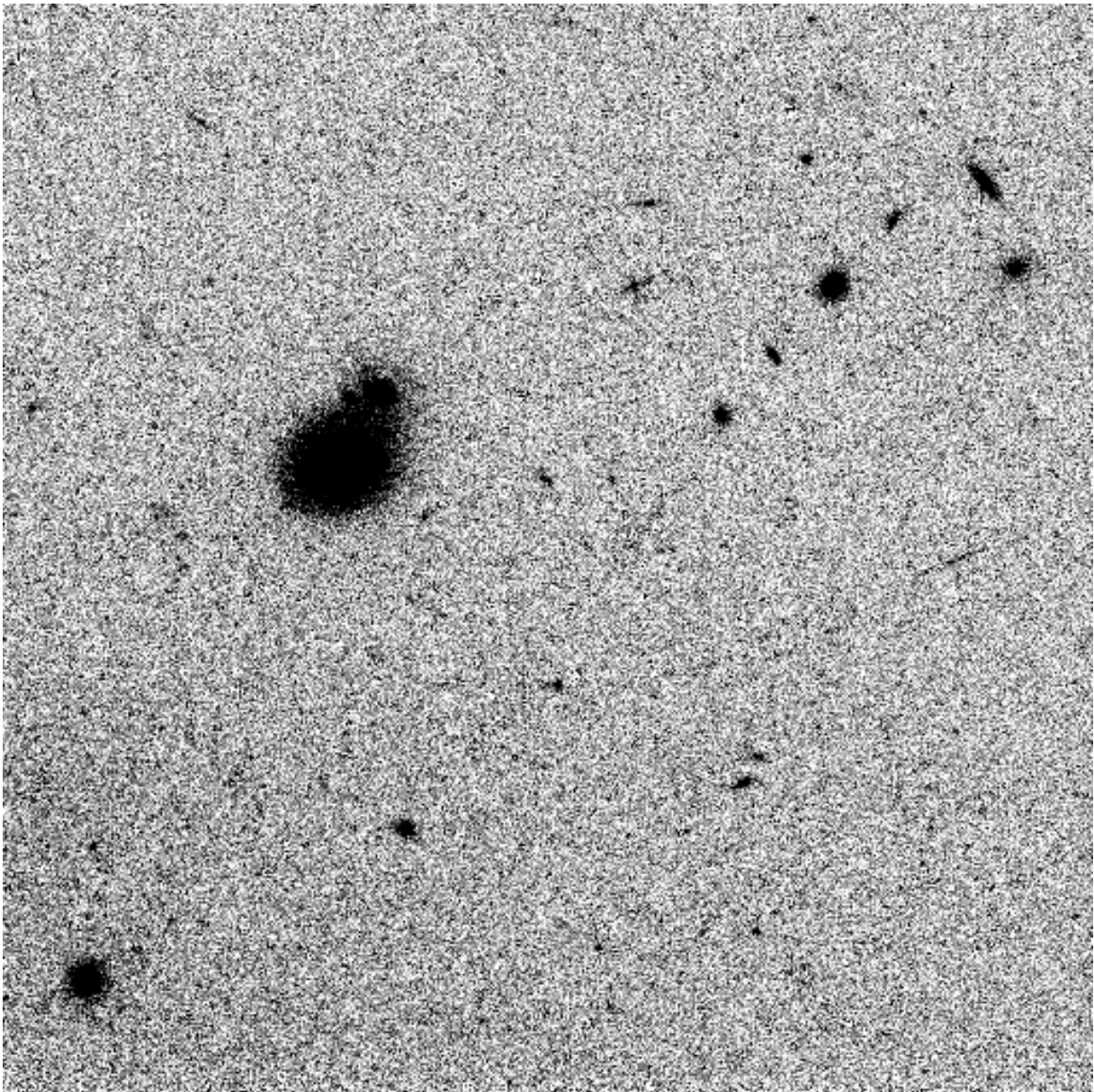


FIG. 2b

of these regions were done so that errors could be determined via statistical bootstrap techniques.

The intrinsic fluctuation signal was found by subtracting, in quadrature, the rms variation of the sky (still in e^-) from that within the constant surface brightness regions. It is precisely the existence of regions of constant surface brightness that encompass several thousand pixels that allows for the fluctuation signal to be measured in such a straightforward manner. That is, the fluctuation signal can be extracted without any need to Fourier-analyze the image to recover the power spectrum, as is traditionally done in studies such as these. As will be shown below, this technique has allowed the fluctuation signal to be measured to high accuracy when it is detected in this manner.

For these observations, the sky background averaged 145–170 electrons, which is well above the readout noise for WFPC2. In the absence of other sources of noise (e.g., filter fluorescence, charge transfer efficiency [CTE] problems, scattered light; see § 4 for details) the only other contribu-

tion to the fluctuation signal besides the galaxy comes from the Poisson noise in the sky background. Division by the average intensity of the constant surface brightness region then gives the fractional luminosity fluctuation, which is presumably driven by a Poisson distribution of red giant stars per pixel. However, there is one small complication that makes this whole procedure a bit less than straightforward, and that is the simple fact that the angular extent of the galaxy (at very faint isophotes) is comparable to the WFPC2 field of view. Examining the outer isophotes from the Las Campanas *I*-band image reveals that, at the maximum radii available for the WFPC2 images ($r = 80''$ for V2L8 and V1L4 and $r = 100''$ for V7L3), the annular surface brightness is 26.85, 28.83, and 27.69 mag arcsec $^{-2}$ for V2L8, V1L4, and V7L3, respectively. This implies that only the light from V1L4 has fallen off enough to render it insignificant (e.g., less than 0.5%) in the calculations of both the sky brightness and its rms variation. For the two other galaxies, 2.5%, and 1.3% of the measured sky value

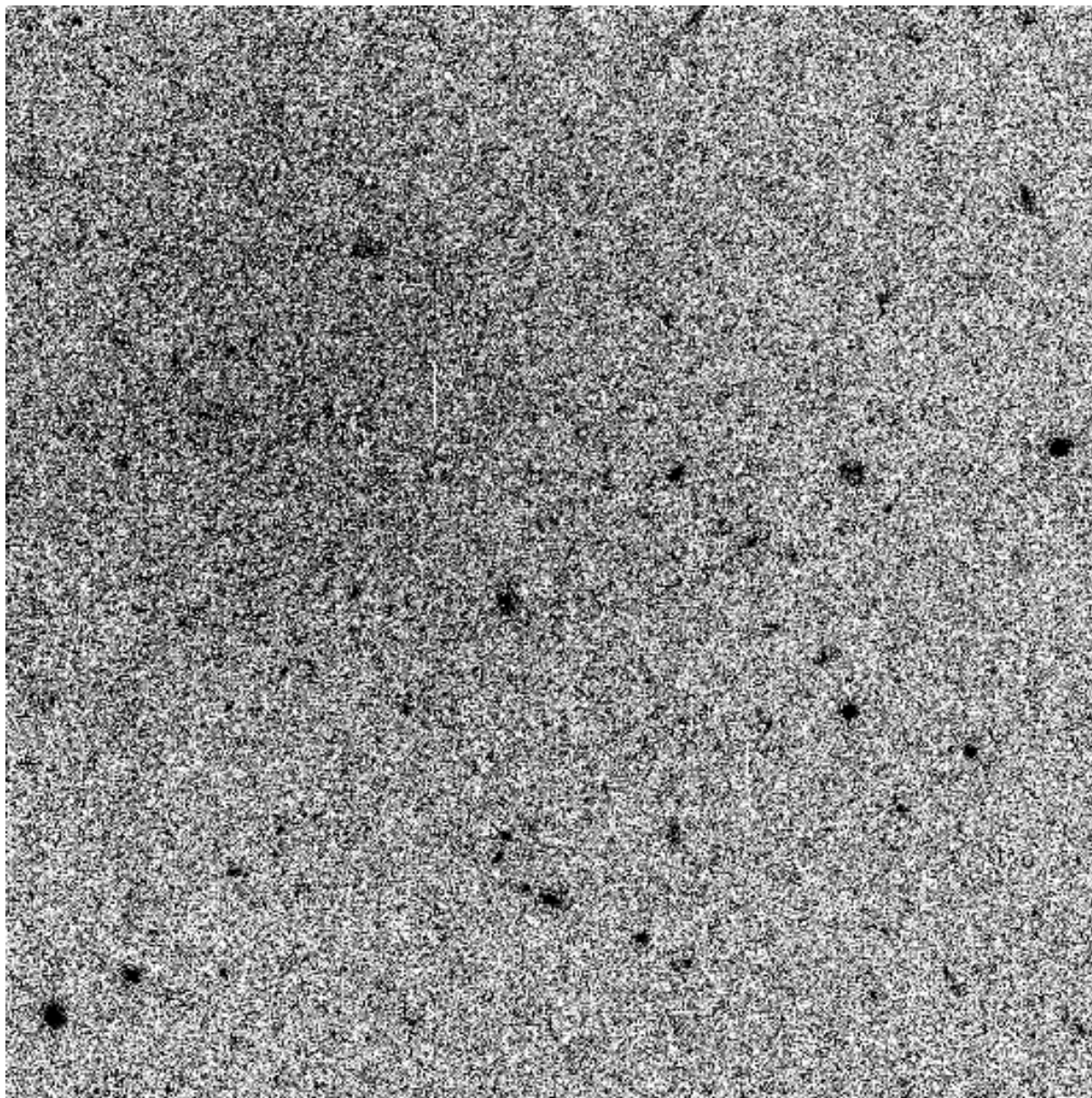


FIG. 2c

is a contribution from the outer stellar light in V2L8 and V7L3, respectively, and needs to be accounted for in the determination of the true sky value.

In the case of sky limited exposures, such as we have, the rms sky error in electrons is

$$\sqrt{(\text{sky intensity}) + (\text{number of exposures}) \times (\text{read noise})^2} \\ = \sigma_{\text{rms}}(\text{sky, in } e^-).$$

If we assume that this rms error represents the true sky noise for all three galaxies [that is, the sky error found is the true $\sigma_{\text{rms}}(\text{sky})$], we can determine the true galaxy rms error using

$$\frac{\sqrt{\sigma_{\text{measured}}(\text{galaxy})^2 - \sigma_{\text{rms}}(\text{sky})^2}}{(\text{galaxy intensity}) - (\text{sky intensity})} = \sigma_{\text{true}}(\text{galaxy}).$$

Uncertainties are dominated by the uncertainty in the numerator. A statistical bootstrap method is used to deter-

mine the uncertainty in the measured values of $\sigma_{\text{measured}}(\text{galaxy})$ and $\sigma_{\text{rms}}(\text{sky})$. These values can be found in Table 2 (see below). In general, $\sigma_{\text{rms}}(\text{sky})$ is larger than the rms of the actual sky counts, in electrons, indicating that readout noise is still a component in the overall noise profile of both the galaxy and sky images.

After grinding through this procedure for all three galaxies, we measure the fractional luminosity fluctuations [$\sigma_{\text{true}}(\text{galaxy})$ above] to be 0.42 ± 0.53 , 0.33 ± 0.05 , and 0.65 ± 0.17 for V2L8, V1L4, and V7L3, respectively. The fluctuation signal for V2L8 clearly is not statistically significant, but to first order the large and statistically significant fluctuation signal measured for V1L4 and V7L3 confirms what was introduced in § 1 (see also Fig. 5 in Bothun et al. 1991).

Combining this measure of the luminosity fluctuations with the probable distance modulus to Virgo yields an estimate for the average magnitude of the stars producing the observed fluctuation (see Tonry & Schneider 1988). Of

course, the distance modulus to Virgo is uncertain, and values of $m - M = 31.0$ – 31.5 remain consistent with the data (see Bothun 1998). Using this range of distance moduli, we can determine the absolute magnitude per pixel for the constant surface brightness regions. For example, in our 2200 s combined exposure, V1L4 has counts of $181.2 \pm 0.8 e^- \text{ pixel}^{-1}$ versus $145.2 \pm 0.3 e^- \text{ pixel}^{-1}$ for the sky or a net count of $36 \pm 0.9 e^- \text{ pixel}^{-1}$, which converts to a mean magnitude per pixel of 28.26 in the Cousins I band ($m = -2.5 \log [(181.2 - 145.2)/7] + 31.26 - 1.22 = 28.26$). The measured fluctuation signal of 0.33 implies that, on average, there are 10 giants per pixel. Using $m - M = 31.0$ then gives $\bar{M}_I = -0.24$. For V7L3, we derive a mean magnitude per pixel of 30.01, with an average of three giants per pixel. This yields $\bar{M}_I = -0.55$. These values are significantly below the typical values of \bar{M}_I found for luminous ellipticals (see below).

3.2. Modeling the Giant Branch

We now have enough information to approximately model the giant branch in terms of a mixture of giants of spectral type K and M, together with an underlying main sequence of A, F, and G (AFG) stars. One way to determine our model is to simply appeal to the calculations of Worthey (1994) in which the fluctuation magnitude is listed for a variety of stellar populations of differing ages and metal abundances. However, those models were developed for application to giant ellipticals, and it is not clear whether they are appropriate for our dE galaxies for the following statistical reason: in a giant elliptical at the distance of the Virgo Cluster, each pixel would contain several hundred giants (and a total of several thousand stars), and thus each pixel represents a statistically reliable realization of the general stellar population. In our case, this is simply not true as each pixel contains a very small number of giants (certainly less than 10 and maybe as few as two), and hence we are subject to discrete effects. In the extreme, part of our fluctuation signal may in fact be driven by the tendency for some pixels to contain zero giants. Thus, we are in a much different counting regime than the case of a giant elliptical.

Nonetheless, we begin with an inspection of the Worthey models. In the I band, \bar{M}_I decreases with increasing metallicity for a fixed-age population. It is only at near-IR wavelengths that the fluctuation magnitude starts to rapidly increase as one gets to more metal-rich populations that contain the cooler, luminous M giants. In addition, throughout the regime of low metallicity ($-2.00 \leq [\text{Fe}/\text{H}] \leq 0.0$), \bar{M}_I is relatively constant. In this metallicity regime, $\bar{M}_I \sim -1.8 \pm 0.1$ over the age range 8–12 Gyr. This is well above the values we found from our data, which are at most $\bar{M}_I \sim -1.0$ for $m - M = 31.5$. So with respect to our data, these models are extremely poor fits in that they achieve $\bar{M}_I \sim -0.5$ only in metal-rich cases, but those populations have $V - I \sim 1.3$ – 1.4 . Conversely, using the bluest $V - I$ models ($V - I = 0.86$, corresponding to $[\text{Fe}/\text{H}] = -2.00$ and an age of 8 Gyr) yield $\bar{M}_I \sim -1.95$. So the comprehensive models of Worthey do not appear to have any applicability to dE galaxies if \bar{M}_I is mostly driven by metallicity variations; we simply cannot even come close to getting consistent values for both $V - I$ and \bar{M}_I .

To make further progress, we model the giant branch by adopting the following procedure: (1) the measured luminosity fluctuation to first order fixes the number of giants

per pixel; (2) we assume that the giant branch can be populated by stars of spectral type K0–M2; (3) we adopt absolute magnitudes and colors for giants as a function of spectral type as shown in Table 3 (not considering types later than M2, as they are typically found in metal-rich bulges, a state far removed from the dE's); and (4) we use the observed $B - V$ and $V - I$ colors as additional constraints that help us to evaluate the contribution of A0–F0 stars to the integrated light.

For a specific demonstration of this procedure, we take the case of V1L4 at an assumed $m - M = 31.0$. The observed fluctuation signal of 33% argues for 10 giants per pixel, to first order. This yields $\bar{M}_I = -0.24$, which is approximately the same as for a K0 giant. Because the observed color of V1L4 is bluer than that of a K0 giant in $V - I$, there clearly is an important contribution from an underlying bluer population. Hence, we seek an approximate model for the giant branch and the ratio of giant branch to AFG stars that can simultaneously satisfy the color and fluctuation signal constraints within the observed errors. These AFG stars represent a blue underlying population that could be a populated main-sequence or a blue horizontal-branch population.

As an example of an acceptable fit, a model (model A) with two A0 and 30 F0 main-sequence stars in combination with two K0, two K2, and two K3 giants returns $\bar{M}_I = -0.30$, $B - V = 0.56$, $V - I = 0.81$, and $m - M = 31.26$. Another model (model B) with three A0 and 40 F0 stars in combination with four K3 giants returns $\bar{M}_I = -0.34$, $B - V = 0.46$, $V - I = 0.75$, and $m - M = 31.31$. Both of these models return distance modulus estimates consistent with cluster membership. In § 6 we will apply the $V - I$ versus \bar{M}_I calibration of Tonry (1991) and Tonry et al. (1997) to uncover widely inconsistent results strongly suggesting that, like the Worthey models, the calibration for giant ellipticals does not hold for these galaxies.

Clearly, given the accuracy of the measurements, we can only come up with only approximate models, but the particular feature we are interested in constraining from these observations is the mean spectral type (effective temperature) of the giant branch. By gauging this, we will have another handle on the metallicity of the stars in these systems. The combination of the observed fluctuation signal and the color does have high constraining power in this regard.

As a further example, we can take model A above and add a 5% (by number) contribution of M2 stars. This yields $\bar{M}_I = -0.97$, $B - V = 0.59$, $V - I = 0.92$, and $m - M = 31.43$. This is not very consistent with the data; in particular, \bar{M}_I is too bright and $V - I$ is marginally too

TABLE 3
STELLAR TYPES USED IN THE MODELS

Stellar Type	M_V	$B - V$	$V - I$	Reference
A0 V.....	+0.7	0.00	0.00	1
F0 V.....	+2.6	+0.27	0.47	1
K0 III.....	+0.7	+1.00	1.00	2, 3
K2 III.....	+0.5	+1.10	1.11	2, 3
K3 III.....	+0.3	+1.18	1.28	2, 3
K5 III.....	-0.1	+1.45	1.53	2, 3
M2 III.....	-0.4	+1.55	1.97	2, 3

REFERENCES.—(1) Allen 1973; (2) Silva 1992; (3) Bessel 1979.

red. To reduce \bar{M}_I while still retaining M2 giants requires the addition of A0 and F0 stars. This addition will make the broadband colors bluer but will also increase the distance modulus, as the absolute magnitude per pixel is now increased. If we double the contribution of F stars, we obtain $\bar{M}_I = -0.79$, $B - V = 0.50$, $V - I = 0.83$, and $m - M = 31.67$. Thus, we can only accommodate a small M star contribution in V1L4 for the largest probably distance modulus to Virgo. For the shorter distance modulus no M giant contribution can be accommodated. Furthermore, none of our models actually can get as blue as $V - I = 0.7$ while being consistent with the derived \bar{M}_I (see Table 2). For instance, using G5 giants can drive $V - I$ down to 0.7, but such models consistently return values for \bar{M}_I that are fainter than we observe (see also Worthey 1994).

3.3. Overall Results

Table 2 lists our overall results in terms of determining \bar{M}_I and its error. All values relevant to the calculation of the fluctuation signal are given in units of electrons per pixel.

The table is laid out as follows: column (1), the galaxy name; column (2), the radius range over which the flat surface brightness profile holds; column (3), the average central surface brightness, through the F814W filter, for the studied regions; column (4), the average central surface brightness, converted to the I band (§ 2.3); column (5), the average galaxy + sky counts within the region defined by column (2), in electrons; column (6), the rms error (σ) for column (5); column (7), the average sky counts for each image, also in electrons; column (8), the rms error (σ) for column (7); column (9), the luminosity fluctuation, from electron counts, determined for each galaxy, followed by an error estimate (detailed in § 4); and column (10), the absolute fluctuation magnitude (\bar{M}_I).

The results of these calculations summarized in this table are clear. The high resolution and low noise of the WFPC2 has allowed for a reliable determination of the luminosity fluctuation signal in two out of three cases. The amplitude of this signal is large for the cases of V1L4 and V7L3 and is likely produced by only 2–10 giant stars per pixel, depending on the types of giants considered.

In Table 4 we list the best-fitting stellar population models to the observed color and fluctuation data. These models were obtained by averaging the results of all models that gave values of $B - V$, $V - I$, and \bar{M}_I that were within the errors in the data and produced a distance modulus in the range $m - M = 31.0$ – 31.7 . No model that we ran got as blue as $V - I = 0.7$. Table 4 is laid out as follows: column (1), galaxy name; column (2), mean spectral type of the giant branch stars; column (3), the K/M giant number ratio, if allowed by the data; column (4), the A + F/K + M stellar ratio; column (5), the distance modulus used; column

(6), the $B - V$ color produced by the models; column (7), the $V - I$ color produced by the models; and column (8), \bar{M}_I , the average I -band magnitude for the stars in the models.

4. ERROR ANALYSIS

The variance, as measured in electrons, is typically 5%–10% higher in the constant surface brightness regions of the dE galaxies compared with the sky background. This is the fluctuation signal, but before we can directly associate that with a Poisson distribution of giant stars per pixel, we must gain a thorough understanding of potential systematic errors arising from the WFPC2 system. These other potential sources of error are as follows:

Dark glow.—This is a nonuniform background that may appear on the WFPC2 chips and is due to luminescence in the MgF₂ CCD windows under cosmic-ray bombardment. Examination for this effect can be done through looking for a small intensity curvature across the sky. This effect is not found in the WFPC2 images discussed in this paper.

CTE errors.—WFPC2 chips experience a CTE loss across the chip of up to 20% along the y -axis. This effect, however, is readily reduced by long exposures and high DN counts. The combined images discussed in this paper are the equivalent of 2200 s images, providing raw (nonaveraged) counts of 2000 DN (14,000 e^-) in a 5×5 pixel box. This reduces the effect of CTE errors from the 20% mark to 2%–3% (see Whitmore 1998). In addition, the majority of the CTE loss occurs at the edges of the chips and can readily be seen in a plot of the average sky counts along a chip column. When this was done on the data discussed herein, it was determined that virtually all of the loss occurred in the 50 pixels at the edges of the chips. These pixels were therefore eliminated from the analyzed image, further reducing any CTE problems to under 0.5%.

S/N loss at the chip edges.—Within approximately 50 pixels of the inner edges of the wide field chips, the S/N drops considerably because of vignetting and spherical aberration as the light is divided between two chips. With the images in question, this effect can be readily eliminated by again examining the sky counts in the chip's inner regions. Eliminating the inner 50 pixels from each image reduced the effects of this problem to zero.

Geometric distortion.—Geometric distortion near the edges of the chips results in a change in the surface area covered by each pixel. In general, this effect is not relevant for surface photometry, where azimuthal averages are taken and the variance in the sky background is determined over areas encompassing thousands of pixels. The flat fields also reduce this problem considerably by boosting the values of the smaller pixels. By analyzing a large number of sky/galaxy regions, each containing a minimum of 25 pixels, we again reduced this effect to under 0.1%.

Scattered light.—Bright stars whose light falls on the planetary camera pyramid mirror can produce an obvious

TABLE 4
BEST-FITTING STELLAR POPULATIONS TO THE OBSERVED PIXEL COLORS
AND LUMINOSITY FLUCTUATIONS

Galaxy	Mean Giant	K/M	A + F/K + M	$m - M$	$B - V$	$V - I$	\bar{M}_I
V1L4.....	K2	∞	4.8	31.28	0.50	0.76	-0.30
V1L4.....	K2	30	5.8	31.45	0.49	0.81	-0.76
V7L3.....	K3.5	∞	6.5	31.36	0.50	0.80	-0.50

artifact on the CCDs, typically in the shape of a large arc. None of the images in this paper suffered from this effect.

Systematic errors.—Potential systematic errors could arise from inappropriate box sizes resulting, in under- or oversampling, the underlying galaxy surface brightness not being constant, and the presence of point sources in the studied region. To counter the first problem, the variance was computed for three different-sized boxes (5×5 , 10×10 , and 15×15 pixels) and the results compared. The weighted differences in sky and galaxy counts between the three box sizes was under 0.2%. To look into the possibility that the studied galaxy regions may not have been flat, a comparison can be done between the counts found in the inner and outer portions of the studied regions. In this case, the errors remain under 0.5%.

The cumulative result of these other effects per statistics box results in a potential additional photometric error of up to 1%–2%. However, our sky and galaxy fluctuation signals and their errors are determined by averaging over approximately 50,000 pixels (in 135 individual boxes) across the WF3 chip, and hence these additional errors are ultimately reduced to well under 1%. The difference in luminosity fluctuation between the sky and the galaxy signals ($\sim 5\%$ – 10%) is well above the level of any possible systematics.

5. THE INDIVIDUAL GALAXIES

The distribution of the giant stars in the inner regions of all three LSB dE's appears to be completely uniform (Fig. 3). There are no apparent clumps or clusters seen at our physical resolution scale of approximately 15 pc. Interestingly, because of the low number of giant stars per pixel, WFPC2 imaging essentially renders these galaxies transparent, and their presence appears only as a “sky fluctuation” (see also Fig. 1). Unless WFPC2 observers are careful, they may well have an object like this in their field without even knowing it.

5.1. V1L4

The ground-based data showed a number of bright regions or clumps in this object. However, it is clear from the higher angular resolution WFPC2 data that these regions are mostly background galaxies shining through V1L4, and hence the underlying structure of V1L4 is quite smooth. The background galaxies are described more fully in another paper (O’Neil, Bothun, & Impey 1999) and demonstrate the transparent nature of this and other dE galaxies. A few other “knots” on the arcsecond scale can be identified that could be localized regions of star formation. Confirmation of this, however, cannot be provided by the F300W filter observations, as those data are extremely noisy.

Analysis of the luminosity fluctuations, described in the last section, shows the typical star within V1L4’s nuclear region to have $\bar{M}_I = -0.32$ to -0.82 ($m - M = 31.0$ – 31.5), which corresponds to spectral types K0 through K2 in the mean. Our models, however, do accommodate the possibility a small M-giant contribution to the fluctuation signal of $K/M = 30$, provided that $m - M = 31.5$. If the luminosity distance is lower, K/M goes to infinity, that is, the possibility of any M-type stars existing within this galaxy goes to zero. Keeping the results consistent with the observed $V - I$ color does not change these results, which equate to 13 ± 1 giant stars in a 10 pc^2 region of the galaxy, of which at most 0.5 could be an M giant star. Figure 3a shows the core of V1L4, with the region of flat surface brightness lying in the

defined annulus. The contour lines in black demark the regions whose brightness is at least 1σ above the mean surface brightness in that region and thus probably are reflective of the actual distribution of the individual giant stars. Interestingly, rather than being evenly distributed throughout the annulus, the majority of the giant stars in this region appear to lie in the southern part of V1L4’s core, accounting for V1L4’s slightly off-center appearance when imaged at coarser angular resolution. In addition, it should be noted that the higher intensity regions do appear to be grouped, indicating perhaps an old stellar cluster now traced by the remnant giant population.

5.2. V2L8

Figures 3b and 3c show the inner regions of V2L8, with the region of constant surface brightness again demarcated by white circles and regions 1σ above the galaxy brightness defined by black contour lines. The distribution of giant-type stars appears to be fairly even throughout the galaxy. Analysis of the luminosity fluctuations of V2L8 outside the nucleated region does not provide a statistically significant result, with $\sigma_{\text{galaxy}} = 0.42 \pm 0.53$. One possible reason for this is that the galaxy completely fills the WFPC2 field of view and no sky measurement is possible. Indeed, inspection of Table 2 shows that the sky counts are significantly higher for this object, although observing conditions (e.g., variable shuttle glow, Sun angle) could also be responsible for these increased counts. Given the strong detection of the fluctuation signal for the other two dE’s in our sample, perhaps this null result indicates that V2L8 is a background galaxy. That might help to explain why it does not conform to the surface brightness–magnitude relation and why it has a nucleus. Recall that a previously nucleated dE in Virgo turned out to be Malin 1 (Bothun et al. 1987).

WFPC2 imaging has clearly resolved the core of V2L8 in the F814W images, although the core drops out entirely in the F300W image. IBM measured $V - I = 1.9$ through a $5''$ diameter aperture. We have reanalyzed the data in attempts to better remove the bad column and remeasure the nuclear colors, but the measurements are quite sensitive to choice of center. Overall, we find colors consistent with the IBM value but can better demonstrate the uncertainty. Based on this, we conclude that the $V - I$ color of the nucleus is 1.85 ± 0.15 mag, which is well within the range defined by luminous ellipticals. Thus, the nucleus of this dE galaxy is extraordinarily red, although the envelope of the galaxy appears to be fairly blue.

But what is the nature of this conspicuous red core? Fitting an $r^{1/4}$ profile gives an effective radius (r_e) of $0''.7$ and an effective surface brightness of $22.0 \text{ mag arcsec}^{-2}$. Its F814W magnitude, as measured through an aperture of diameter $2''$, is ~ 22.8 . If V2L8 is in the Virgo Cluster, then this nucleus is, in fact, an extremely small scale bulge with $r_e \sim 50 \text{ pc}$ and has an absolute magnitude at Cousins I of -10 to -10.5 , consistent with its being a bright, very metal-rich globular cluster (perhaps similar to those seen in NGC 5128; Frogel 1984). Given the extremely diffuse nature of the central regions of this object, the formation of a highly compact bulge is very curious. If true, this is the first identified $r^{1/4}$ component of a dE galaxy with such a small scale length. The red color further suggests a metal-rich giant population. Attempts at spectroscopy of this nucleus in 1998 February using the now-defunct MMT were unsuccessful because of weather and difficulty in finding

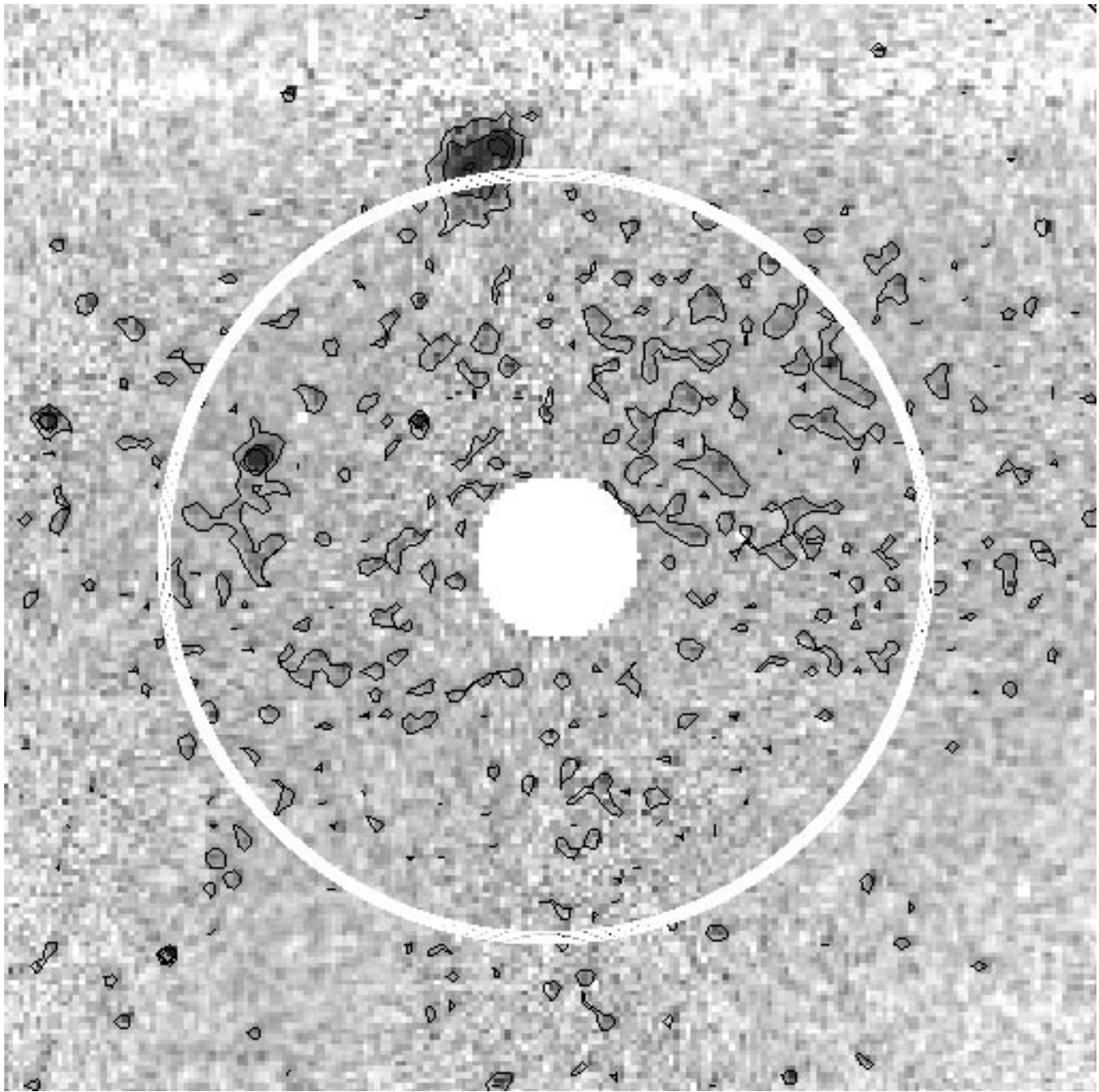


FIG. 3a

FIG. 3.—Gray-scale images of the central regions of the three galaxies in this study: (a) V1L4, (b) and (c) V2L8, and (d) V7L3. White circles demarcate the inner and outer edges of the constant surface brightness regions for each galaxy, and black contour lines encircle the regions 1σ above the sky level. All the images are $20''$ across, except for (b), which shows the core of V2L8. To allow for comparison between images, a section of V2L8 (shown by a black box in b) that is $20''$ across is shown in (c). Note that these figures show the mosaicked images and are being shown for demonstration of the studied areas only. Mosaicked images were not used for the data analysis.

the nucleus on the acquisition TV. The lack of an observed fluctuation signal, however, has renewed our quest for optical spectroscopy as this object may be background and, like Malin 1, intrinsically large.

5.3. V7L3

The WFPC2 images show V7L3 to have a very even stellar distribution, with even its core hardly brighter than the sky background. Remarkably, even with the WFPC2

image (additively) binned in 10×10 pixels (giving the image a resolution of $1'' \text{ pixel}^{-1}$), V7L3 is still a fairly diffuse blob within the sky image and is quite difficult to identify. The observed fluctuation signal is relatively large (because of its lower surface brightness compared with V1L4) and is consistent, to first order, with a stellar population of only three giants per pixel, yielding $\bar{M}_I = -0.56$ to -1.06 , or spectral type K2/K3. This is a slightly later spectral type than the case of V1L4, even though both dE's have the same

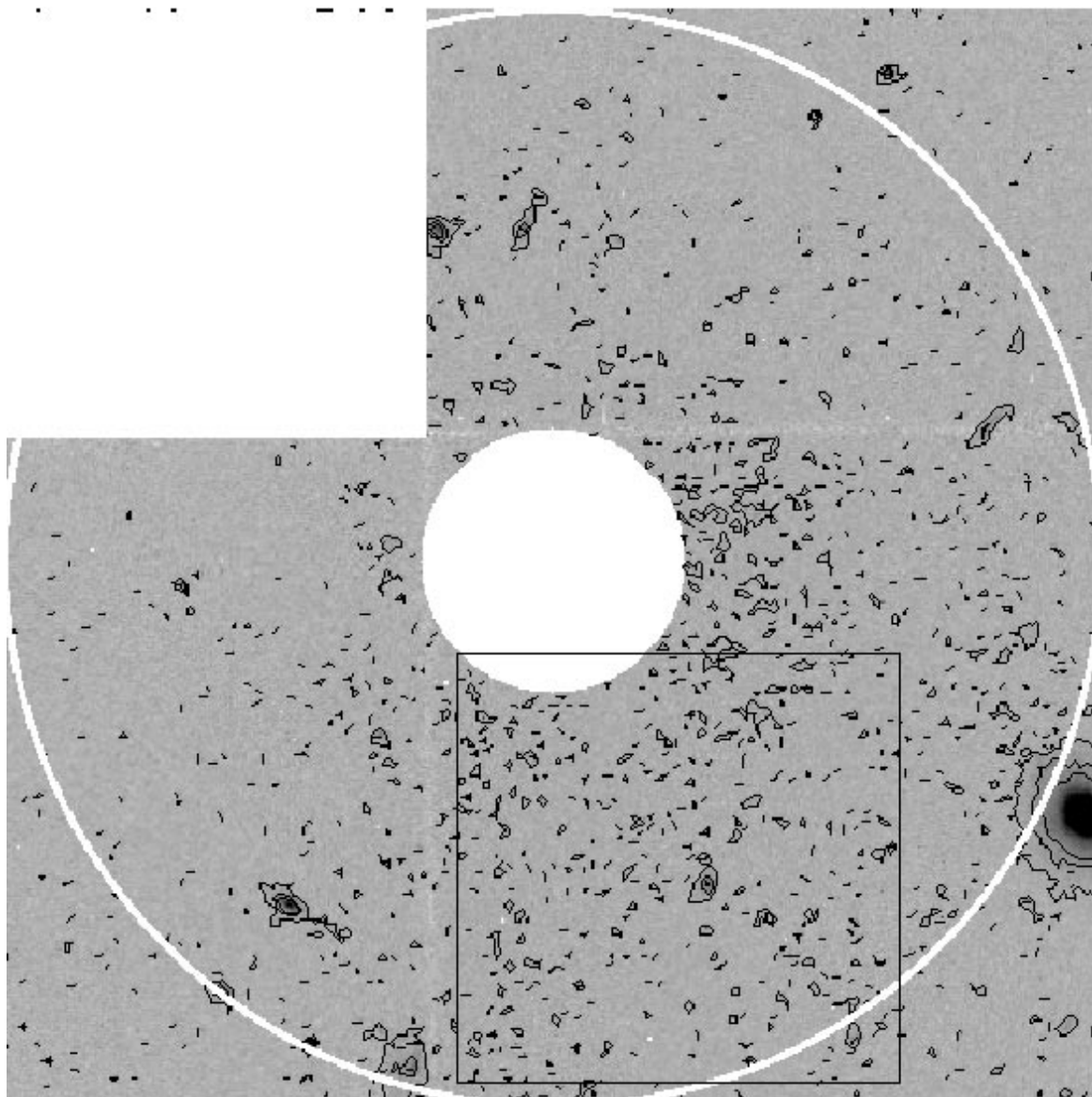


FIG. 3b

$V-I$ color. To accommodate this requires a large contribution, per pixel, from the underlying A and F stars (mostly F stars). However, it is clear that the data cannot accommodate M giants (which have $M_I \sim -2.4$), as the model quickly gets too red. Moreover, the absolute magnitude per pixel in the center regions is fainter than the absolute I -band magnitude of an M2 star, which would lead to fluctuations that are larger than we observe. In fact, it is very difficult to fit any one of our seven component models to the data for this galaxy at the short distance modulus. Successful models tend to be absurd (a point noted earlier by Bothun et al. 1991 regarding the colors of some of these dE's) and require approximately equal mixtures of A0 main-sequence stars and K giants. For instance, model C has equal numbers of A0 and K3 stars (and nothing else), and this returns $\bar{M}_I = -0.74$, $B-V = 0.54$, $V-I = 0.85$, and $m-M = 31.12$. Adding 10 times as many F stars to this model produces $\bar{M}_I = -0.88$, $B-V = 0.45$, $V-I = 0.82$, and pushes $m-M$ to 31.70. Once again, it is essentially

impossible to push these models as blue as $V-I = 0.70$ while simultaneously reproducing the observed \bar{M}_I .

Because the composite giant branches appear to be similar, the more diffuse nature of V7L3 relative to V1L4 must be due directly to a lower surface density of giants or, equivalently, an increased average spatial separation between giant stars. The physical cause of this is unclear. Figure 3d shows the core of V7L3 with the regions 1σ above the galaxy brightness demarcated by black contour lines. Figure 3d shows V7L3 to have the most even distribution of giant stars of the three galaxies in this study. This even stellar distribution within V7L3's core, combined with the circular appearance of the galaxy and the lack of any large stellar knots within V7L3, argues for the idea that LSB galaxies are diffuse and low surface brightness by nature and are not due to outside influences that might cause the galaxies to "puff up" in some stochastic manner. Under that scenario, one might expect there to be considerably more clumpiness in the stellar distribution than we

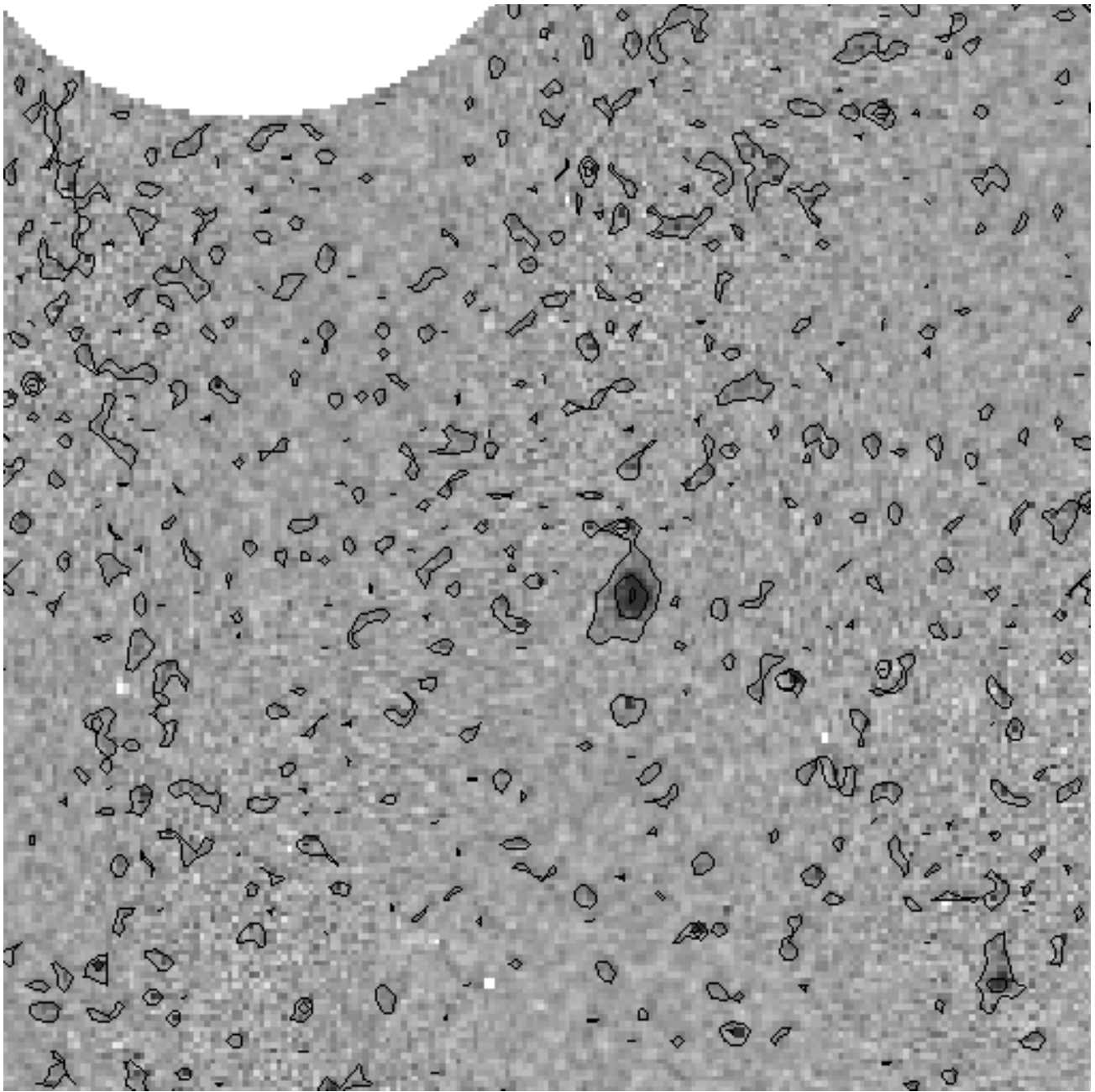


FIG. 3c

actually observe, which in all three cases is consistent with an old, dynamically relaxed distribution of giant stars.

6. DISCUSSION

The primary result of this study is the firm detection of luminosity fluctuations that are associated with a small number of giants per pixel in two of the three LSB dE galaxies in our sample. Specifically, luminosity fluctuations of the inner, constant surface brightness regions yields a density of 2–10 red giants per pixel for two of the imaged galaxies. Because the distance to Virgo is relatively well known, we can use the measured fluctuation signal, in combination with the observed $V-I$ color, to constrain the respective contributions of K and M giants to the observed light. In so doing, the result is clear. We cannot simulta-

neously account for the observed fluctuation signal and the very blue $V-I$ in any model that has an M giant contribution. In fact, the models strongly favor very early K giants and hence a relatively warm effective temperature for the composite giant branch. This implies that the population is relatively metal-poor.

In more general terms, we find that it is extremely difficult for any model to reach $B-V \sim 0.5$ with $V-I$ as blue as 0.7 and still exhibit an \bar{M}_I brighter than -0.3 . This is relatively easy to understand, as to achieve such blue colors requires the addition of many F stars (main-sequence or blue horizontal-branch stars), which greatly increases the number of stars per pixel and lowers the overall fluctuation signal. So, in this sense, the stellar populations of these blue LSB dE galaxies remain mysterious and ill-constrained.

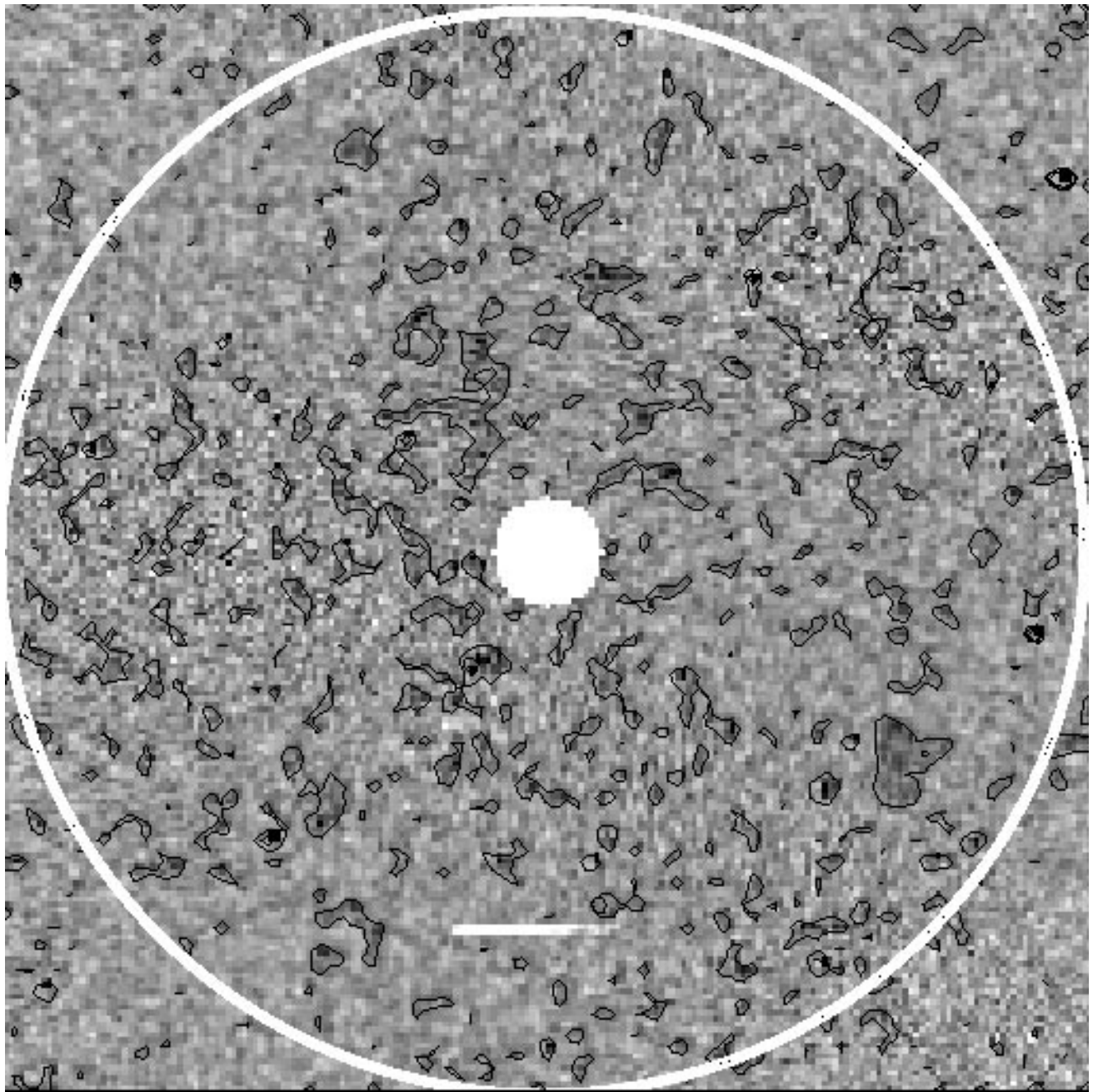


FIG. 3d

This has been noted as far back as Bothun & Caldwell (1984) and is a manifestation of the basic dilemma involved in trying to produce galaxies with $B - V \sim 0.5$ that have no active star formation and very low surface brightness. The most confident statement we can make from the fluctuation data, is that the giant branch is likely devoid of a significant population of M stars.

We can, of course, turn the situation around and derive the distance to the Virgo Cluster. Two calibrations are available for this purpose. Tonry (1991) gives

$$M_I(\text{Cousins}) = -4.84 + 3.0(V - I),$$

based on a sample that includes colors as blue as $V - I = 0.85$. The revision of this calibration, by Tonry et al. (1997), based on including very red galaxies (and strictly

valid only over the range $1.00 \leq V - I \leq 1.30$) is

$$M_I(\text{Cousins}) = -1.74 + 4.5[(V - I) - 1.15].$$

For V1L4, we derive $\bar{m}_I = 30.76$, and for V2L3 we get $\bar{m}_I = 30.45$. Both dE's have $V - I = 0.7 \pm 0.1$. The Tonry (1991) calibration thus yields $m - M = 33.3 \pm 0.3$ for the two galaxies averaged. The Tonry et al. (1997) calibration results in a distance modulus 1 mag farther. If we believed these calibrations, then these objects are clearly not in the Virgo Cluster. However, this is more likely indicating that the metallicity-driven variation in \bar{M}_I , which is at the heart of the calibration (and the Worthey models), simply does not apply to LSB dE's, possibly because of discrete effects. At some level, the actual surface brightness (e.g., the number of stars per pixel) becomes important. Consider the extreme

case where either the surface brightness is sufficiently low or the pixel size is sufficiently small that, on average, there is only one giant per pixel. Now the surface density of giants is 1 ± 1 , and the fluctuation signal would be 100%. In this limit, it is not clear that the \bar{M}_I versus $V-I$ calibration means anything, because the dominant driver of the fluctuation signal is the fact that some pixels would have zero giants in them. The case of V7L3, where we derive a surface density of giant stars of ~ 3 per 10 pc^2 , is close to this limit.

Of course, in this limit, the color fluctuations on the pixel scale would also be very severe. We had hoped to measure this effect with the combination of the F300W and F814W filters but were effectively thwarted by the low S/N in the F300W case. Without this additional information, our constraint on the stellar population per pixel is limited, and all we can really do is focus on the relative contributions of K versus M giants. In general, we find that we cannot simultaneously produce the inferred pixel density of giants and the observed $V-I$ color with any model that includes M giants. Another way to state this is by again comparing our results with the models of Worthey (1994). Whereas it is possible to match our observed spectral fluctuations with Worthey's predictions, our galaxies still remain significantly bluer in $V-I$ than the model predicts. Because the redder colors of Worthey's models are due in large part to the presence of late K and M giant stars, this offers further evidence against a significant population of such stars within V1L4 and V7L3. The apparent paucity of these stars is likely an indication that these dE galaxies are relatively metal-poor.

For the case of V2L8, we did not detect a fluctuation signal. While this may be due to its large angular extent on the WF3 frame, it might also indicate that V2L8 is background to Virgo. If indeed V2L8 is in the Virgo Cluster, then we have discovered what is likely the smallest bulge measured to date, having an effective radius of only 50 pc.

This bulge is quite red (as red as giant ellipticals) and thus may well be substantially more metal-rich than the rest of the galaxy. Possibly, it is a signature of a secondary star formation event that occurred over a very small spatial scale. To date, no other dE LSB galaxy that has been studied shows such a very small, very red core. Clearly, spectroscopy of this core is desirable. Either we have a very small bulge here, or V2L8 is in the background and may therefore be like Malin 1: a LSB object with an L^* , metal-rich bulge (see Impey & Bothun 1989).

Finally, we comment on the LSB nature of these objects. We find no evidence for small-scale clumping of stars on the 10–20 pc spatial scale. To first order, this suggests that these systems are dynamically relaxed. Expansion of these systems is then unlikely to be the explanation for their observed low surface brightnesses. Because we have detected surface brightness fluctuations coming from a very small number of stars per pixel, we know that individual giant stars are dominating the light per pixel. Thus, their LSB nature is also not caused by an absence of giant light. While this is not a surprising result, this study is the first to demonstrate that directly. This leaves the physical separation between individual giant stars as the cause of the observed low surface brightnesses. In the WFPC2 data, such low-density galaxies could easily be dismissed as “sky noise” and remain undetected. The continuing difficulty to detect faint, LSB galaxies with any instrumentation has clear implications for reliable determinations of the faint end slope of the galaxy luminosity function.

We acknowledge *HST* award GO-05496 to help support data acquisition and reduction. We also acknowledge NSF support for low surface brightness galaxy research at the University of Oregon. Conversations with Harry Ferguson on the general subject of luminosity fluctuations have greatly improved our understanding of the subject.

REFERENCES

- Allen, C. 1973, *Astrophysical Quantities* (3d ed.; London: Athlone)
- Bernstein, G. M., Nichol, R. C., Tyson, J. A., Ulmer, M. P., & Wittman, D. 1995, *AJ*, 110, 1507
- Bessell, M. S. 1979, *PASP*, 91, 589
- Binggeli, B., Sandage, A., & Tarengi, M. 1985, *AJ*, 90, 1681
- Bothun, G. D. 1998, *Modern Cosmological Observations and Problems* (London: Taylor & Francis), chap. 2
- Bothun, G. D., & Caldwell, C. N. 1984, *ApJ*, 280, 528
- Bothun, G. D., Caldwell, N., & Schombert, J. 1989, *AJ*, 98, 1542
- Bothun, G. D., Impey, C. D., & Malin, D. F. 1991, *ApJ*, 376, 4
- Bothun, G. D., & Mould, J. R. 1988, *ApJ*, 324, 123
- Bothun, G. D., Mould, J. R., Caldwell, N., & MacGillivray, H. T. 1986, *AJ*, 92, 1007
- . 1987, *AJ*, 94, 23
- Bothun, G. D., Mould, J. R., Wirth, A., & Caldwell, N. 1985, *AJ*, 90, 677
- Brodie, J. P., & Huchra, J. P. 1991, *ApJ*, 379, 157
- Caldwell, C. N. 1987, *AJ*, 94, 1116
- Caldwell, C. N., & Bothun, G. D. 1987, *AJ*, 94, 1126
- Caldwell, N., Armandroff, T. E., Da Costa, G. S., & Seitzer, P. 1998, *AJ*, 115, 535
- Cawson, M. 1983, Ph.D. thesis, Univ. Cambridge
- Conselice, C., & Gallagher, J. 1998, *MNRAS*, 297, L34
- de Blok, W. J. G., & McGaugh, S. S. 1997, *MNRAS*, 290, 533
- Dekel, A., & Silk, J. 1986, *ApJ*, 303, 39
- Durrell, P., et al. 1996, *AJ*, 112, 972
- Ferguson, H. C. 1991, *BAAS*, 23, 1338
- Ferguson, H. C., & Binggeli, B. 1994, *A&A Rev.*, 6, 67
- Frogel, J. 1984, *ApJ*, 278, 119
- Held, E. V., & Mould, J. R. 1994, *AJ*, 107, 1307
- Impey, C., & Bothun, G. 1989, *ApJ*, 341, 89
- Impey, C., Bothun, G., & Malin, D. 1988, *ApJ*, 330, 634 (IBM)
- Jerjen, H., & Dressler, A. 1997, *A&AS*, 124, 1
- Jerjen, H., Freeman, K. C., & Binggeli, B. 1998, *AJ*, 116, 2873
- Kepner, J. V., Babul, A., & Spergel, D. N. 1997, *ApJ*, 487, 61
- Knezek, P. M., Sembach, K. R., & Gallagher, J. S. 1997, *A&AS*, 191, 8108
- Kormendy, J. 1985, *ApJ*, 295, 73
- . 1987, *Proc. Eighth Santa Cruz Summer Workshop in Astronomy and Astrophysics* (New York: Springer), 163
- Lee, M. G., Freedman, W. L., & Madore, B. F. 1993, *AJ*, 106, 964
- McGaugh, S., Schombert, J., & Bothun, G. 1995, *AJ*, 109, 2019
- Meurer, G. R., Mackie, G., & Carignan, C. 1994, *AJ*, 107, 2021
- Meylan, G., & Prugniel, P., eds. 1994, *Dwarf Galaxies*. (Garching: ESO)
- O'Neil, K. 1997, Ph.D. thesis, Univ. Oregon
- O'Neil, K., Bothun, G., Impey, C., & McGaugh, S. 1998, *AJ*, 116, 657
- . 1999, *ApJS*, submitted
- Peterson, R. C., & Caldwell, N. 1993, *AJ*, 105, 1411
- Reed, B. C., Hesser, J., & Shawl, S. 1988, *PASP*, 100, 545
- Sage, L. J., Salzer, J. J., & Loose, H.-H. 1992, *A&A*, 265, 19
- Sandage, A., & Binggeli, B. 1984, *AJ*, 89, 919
- Secker, J., & Harris, W. E. 1996, *ApJ*, 469, 623
- Secker, J., Harris, W. E., & Plummer, J. D. 1997, *PASP*, 109, 1377
- Silk, J., Wyse, R. F. G., & Shields, G. A. 1987, *ApJ*, 322, L59
- Silva, D. 1992, Ph.D. thesis, Univ. Michigan
- Spaans, M., & Norman, C. A. 1997, *ApJ*, 488, 2
- Sung, E.-C., et al. 1998, *ApJ*, 505, 199
- Tonry, J. 1991, *ApJ*, 373, L1
- Tonry, J., et al. 1997, *ApJ*, 475, 399
- Tonry, J., & Schneider, D. P. 1988, *AJ*, 96, 807
- Ulmer, M. P., Bernstein, G. M., Martin, D. R., Nichol, R. C., Pendleton, J. L., & Tyson, J. A. 1996, *AJ*, 112, 2517
- Vader, J. P. 1987, *ApJ*, 317, 128
- Vader, J. P., & Chaboyer, B. 1994, *AJ*, 108, 1209
- Whitmore, B. 1998, *WFPC2 Photometry Cookbook* (Baltimore: STScI)
- Worthey, G. 1994, *ApJS*, 95, 107
- Young, C., & Currie, M. 1995, *MNRAS*, 273, 1141